The oxygen reduction reaction on Pt overlayers deposited onto a gold film: ligand, strain and ensemble effect.

Yu-Jia Deng[1], Vladimir Tripkovic[1,2], Jan Rossmeisl[1] and Matthias Arenz[1]*

1. Nano-Science Center, Department of Chemistry, University of Copenhagen, Universitetsparken 5, DK-2100 Copenhagen Ø, Denmark

2. Department of Energy Conversion and Storage, Technical University of Denmark, DK-4000 Roskilde, Denmark

Corresponding author: M. Arenz (m.arenz@chem.ku.dk)

Phone: +45-35320002; **Fax**: +45 35320322

Abstract

We study the oxygen reduction reaction (ORR), the catalytic process occurring at the cathode in fuel cells, on Pt layers prepared by electrodeposition onto an Au substrate. Using a nominal Pt layer by layer deposition method previously proposed, imperfect layers of Pt on Au are obtained. The ORR on deposited Pt layers decreases with increasing Pt thickness. In the sub-monolayer region, however, the ORR activity is superior to that of bulk Pt. Using density functional theory (DFT) calculations, we correlate the observed activity trend to strain, ligand and ensemble effect. At sub-monolayer coverage certain atom configurations weaken binding energies of reaction intermediates due to a ligand and ensemble effect, thus effectively increasing the ORR activity. At higher Pt coverage the activity is governed by a strain effect, which lowers the activity by decreasing the

oxidation potential of water. This study is a nice example of how the influence of strain, ligand and ensemble effect on the ORR can be deconvoluted.

1. Introduction

Proton exchange membrane fuel cells (PEMFCs) powered by hydrogen are promising devices for clean and efficient energy conversion [1]. They are especially useful for high power mobile applications like cars, which require a certain operation capacity (driving range) [2]. Recently the first commercial fuel cell powered cars have been introduced to the consumer market. While a gradual increase in the number of PEMFC powered cars can be expected in the next years, a large-scale production still faces significant challenges. Most of these challenges are related to the cathode catalyst that converts oxygen to water, *via* the oxygen reduction reaction (ORR). The current electrocatalysts of choice for PEMFCs are all Pt based. The scarcity of Pt, however, requires that for mass production the amount of Pt is considerably reduced [2]. Short and medium term strategies for facing this challenge are the activity improvements of Pt by alloying with one or more other components, thus increasing the activity and at the same time reducing the Pt content, applying core-shell catalysts, where only the catalyst shell consists of Pt, nanostructured thin film catalysts, or nanoframes [3]; whereas long term strategies include the complete removal of Pt and other precious metals [4].

For the Pt based strategies the activity increase is usually assigned to electronic strain and/or ligand effect [5]. Separation between these effects can be difficult, but investigations often point towards the strain effect being predominant due to leaching of the solute element. Here we investigate ORR on Pt overlayers deposited onto an Au substrate. Such a system can be regarded as a model for core-shell catalysts. Pt overlayers under tensile strain should be less active catalysts compared to bulk Pt since they will be more prone to surface poisoning by water oxidation products. A recently proposed experimental protocol for layer by layer Pt deposition onto an Au substrate

allows for a systematic investigation of the activity of the thin films as a function of Pt thickness[6]. Using this experimental protocol in combination with Density Functional Theory (DFT) calculations, we show that the strain effect is not always controlling the ORR activity, particularly in the Pt sub-monolayer region where the ligand effect leads to an activity increase for certain thin film compositions.

2. Experimental

2.1. Preparation of Au-films onto glassy carbon electrodes

PtAu-film electrodes were prepared in several steps. First, an Au-film was deposited onto glassy carbon (GC) onto which in the second step Pt was electrodeposited in a nominal layer by layer fashion. For the first step a standard GC electrode (d=9mm) was polished successively with 1µm and 0.3µm Al_2O_3 powder and thereafter cleaned in an ultrasonic bath; first in Millipore water (18.2MΩ cm^{-2}), then in acetone, ethanol and finally in isopropanol. Thereafter the GC electrode was dried under a N_2 flow and subjected to an O_2 plasma to clean the surface further. Finally a 5nm Ti interlayer was deposited (0.7Å/s) in a thermal evaporator (Auto 306, Edwards) followed by a 100nm Au film (0.7 Å /s). After deposition, the Au film was characterized by atomic force microscopy (AFM) in tapping mode using a Veeco Multimode 8 microscope.

2.2. Electrochemical preparation of PtAu-film electrodes and oxygen reduction reaction measurements

All electrochemical experiments were carried out in three-compartment electrochemical cells made out of Teflon, where the reference electrode (RE) compartment was separated from the working electrode (WE) compartment by a membrane [7]. A saturated calomel electrode (SCE) and a Pt mesh were used as the RE and counter electrode (CE), respectively. In all measurements we compensated for the solution resistance by using the potentiostat`s (ECI-200 from Nordic Electrochemistry) analog feedback scheme. The effective solution resistance was around 2 Ω, online determined by

superimposing an AC signal (5 kHz, 5 mV). For obtaining a PtAu-film electrode, the prepared Au-film was inserted into a rotating disk electrode (RDE) tip, and Pt was electrodeposited onto the electrode in a nominal layer by layer fashion using an electrochemical cell containing 0.5 mol/L NaCl and 3 mmol/L K_2PtCl_4. The layer by layer deposition was adapted from ref.[6] confirming the potentials of Pt deposition, its suppression and hydrogen underpotential deposition (H_{upd}) removal, see Fig. S1. After immersion of the Au film electrode, the potential was held for 2 seconds at 0.4 V_{SCE} and then the potential was jumped for 15 s to -0.8 V_{SCE} to deposit platinum onto the Au surface. Finally, the potential was jumped for 30 s back to 0.4 V_{SCE} to clean the surface. It is reported in literature that with this procedure a monolayer of Pt is deposited onto Au (see discussion below). To obtain Pt multilayers, the procedure was repeated as many times as the number of nominal Pt layers.

The basic electrochemistry (cyclic voltammetry) and ORR were measured in a separate cell containing 0.1M $HClO_4$ electrolyte, which was prepared from conc. $HClO_4$ (Suprapur grade) and Millipore water. The ORR activity was determined for each layer. After deposition of a Pt layer, the electrode was carefully rinsed with Millipore water and then transferred into a cell containing oxygen saturated 0.1M $HClO_4$. In order to characterize the electrode at first a cyclic voltammogram (CV) was recorded applying a fast scan rate of 1 V/s to suppress ORR currents, and thereafter the ORR was determined using a scan rate of 50 mV/s and a rotation rate of 1600 rpm.

2.3. Density functional theory calculations

Total energies are calculated using DFT calculations employing a grid-based projector-augmented wave method (GPAW) code integrated with Atomic Simulation Environment (ASE) [8]. Calculations are performed using the RPBE exchange-correlation functional [9] and a grid spacing of 0.18 Å. The RPBE relaxed lattice constants of Pt and Au are 3.991 and 4.186 Å, respectively. The occupation of

one-electron states is calculated at an electronic temperature of k_BT = 0.1 eV, and then all energies are extrapolated to k_BT = 0 K.

Polycrystalline thin films are modelled using low Miller index (111), (110) and (100) surface terminations. These planes have the lowest surface free energies and thus are expected to dominate the thin film surface. Pt and Au electrodes are made of 6 layers periodically repeated in two surface directions and with at least 10 Å vacuum separation in the surface normal direction. The bottom two layers are fixed, while remaining atoms and adsorbates are allowed to relax in order to assume minimum energy positions. The surface unit cell for the (111) plane is $(\sqrt{3}x\sqrt{3})R30^{o}$. The unit cell has three atoms in each layer, allowing the composition to be varied in increments of 1/3 ML. The surface size of the (100) unit cell is 1x2, having 2 atoms in each layer. For (110) we used a 1x2 missing row reconstructed cell, with 4x2 surface atoms. Cartoons of the different electrodes are shown in the ESI. Brillouin zones of (111), (110) and (100) surfaces are sampled by (4x4x1), (4x2x1) and (3x2x1) Monkhorst–Pack k-point grids,[10] whose densities are sufficient to obtain converged results. Convergence was reached when the sum of absolute forces acting on atoms becomes less than 0.05 $eV\text{Å}^{-1}$.

To investigate activity of thin films with the 1-2 nominal layer thickness, the composition is varied in the two surface layers by substituting Au atoms in a pure Au slab for Pt. For thicker films, activity was measured by successively substituting 1-5 Au layers with Pt layers.

3. Result and discussions

We start with the discussion of the Au-films deposited onto GC RDE tips. The roughness of the obtained Au-films was analyzed using AFM. Figure 1 shows typical AFM images in two length scales, i.e. (a) in low and (b) in high magnification. It can be seen that the Au-film is homogeneous and completely covers the GC tip. The film consists of individual grains in the size range of about 90 nm, which are relatively smooth. The inset in Figure 1 demonstrates that the electrochemical

response of the Au-film in cyclic voltammetry is as expected and consistent with previous works by other groups[11]. These characterizations confirm that a uniform, flat Au-film is deposited onto the GC tips. The Au coated GC tip is a good substrate for electrochemical Pt deposition, which was the next step in our investigation.

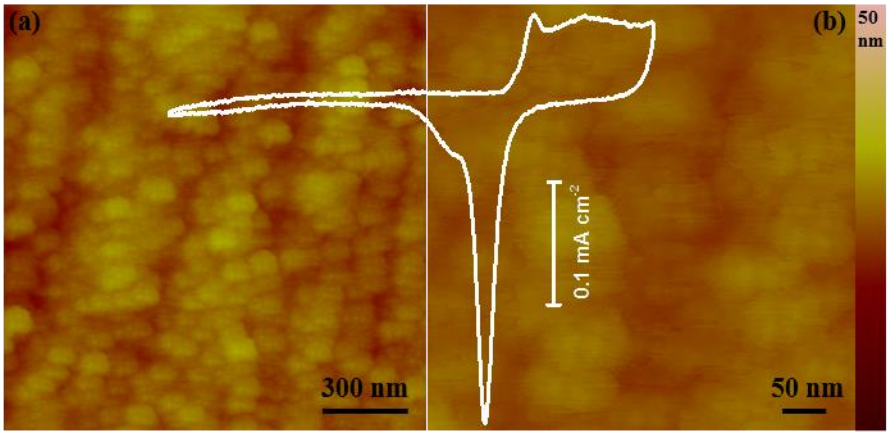

Figure 1. (a) and (b) AFM images of Au Film, and the inset shows a representative CV we obtained for Au-film electrode. The CV was recorded in 0.1M $HClO_4$ electrolyte saturated with Ar; the potential limits are -0.1 to 1.35V_{SCE}, the scan speed was 50 mV/s.

In Figure 2, the inset presents the experimental protocol reported to lead to layer by layer deposition of a Pt film onto gold, see [6]. After immersion of the Au-film electrode into 0.5 mol/L NaCl electrolyte containing 3 mmol/L K_2PtCl_4, first the potential is held for 2 seconds at 0.4 V_{SCE} in order to clean the surface, and thereafter jumped to -0.8 V_{SCE} for 15 s to deposit the first Pt layer. The deposition is completed by returning the potential back to 0.4 V_{SCE} for 30 s. The individual potentials were chosen according to a CV shown in Figure S1, which displays Pt deposition onto an Au-film electrode by scanning the potential with a rate of 2 mV/s in 0.5 mol/L NaCl containing 3 mmol/L K_2PtCl_4. At 0.4 V_{SCE}, there is no Pt deposition reaction apparent as the current is zero, whereas at -0.8 V_{SCE}, the overpotential is high enough to deposit Pt ultrafast and consecutively cover its surface with hydrogen atoms which prevents further deposition [6]. Stepping the potential

back to 0.4 $V_{SCE,}$ the adsorbed hydrogen is removed and additional Pt layers (Pt multilayer films) can be deposited by repeating the procedure.

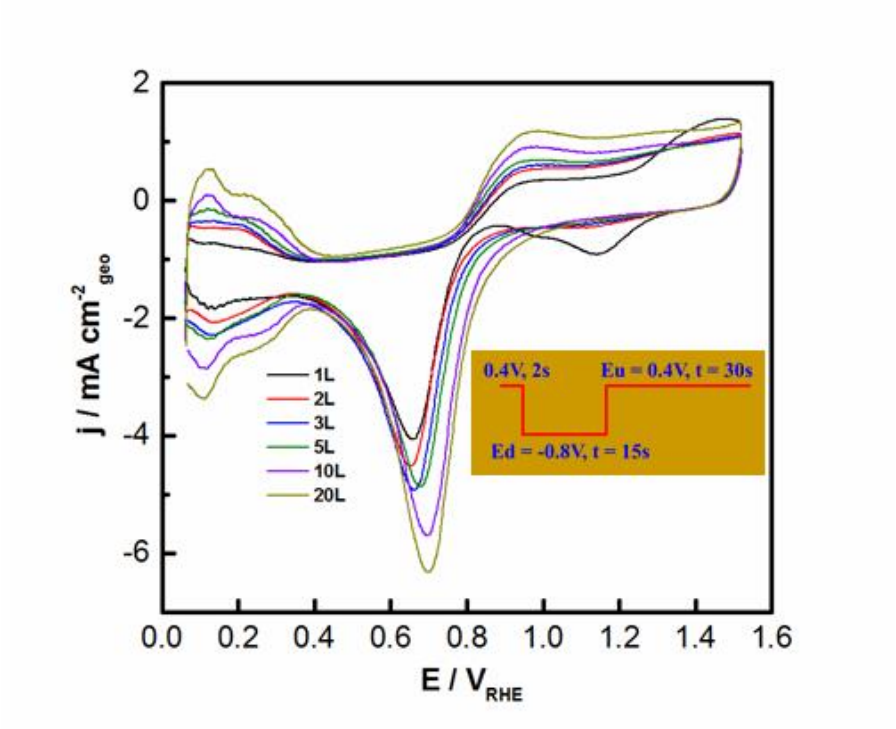

Figure 2. CVs as function of nominal number of Pt layers deposited onto the Au-film according to the procedure indicated in the insert: first the potential jumps from 0.4 to -0.8 VSCE (indicated as Ed) to deposit Pt; after 15 s the potential jumps back to 0.4 VSCE (Eu) and is held for 30 s to clean the surface from adsorbed hydrogen; the deposition procedure was done in 0.5 mol/L NaCl electrolyte containing 3 mmol/L K_2PtCl_4. The CVs were obtained in a separate cell containing O_2 saturated 0.1M $HClO_4$ electrolyte scanning with a rate of 1V/s.

After depositing a Pt layer onto the Au film, the electrode was carefully rinsed in Millipore water and transferred into a separated cell containing 0.1M $HClO_4$ electrolyte. The strategy was to limit the time and number of cycles between electrochemical characterization (CV) and activity determination (ORR polarization curves). Therefore, the electrolyte was already saturated with O_2 upon immersion and only a few, fast (1 V/s scan rate) cycles were recorded in the potential window between 0.05 and 1.5 V_{RHE} to probe the deposited Pt film, see Figure 2. From the reduction peak in the CV at ca. 1.2 V_{RHE} it can be seen that after the deposition of one nominal Pt monolayer onto the

Au-film, there are still some areas on the electrode with Au surface atoms exposed to the electrolyte. After the deposition of the second Pt layer, all gold features disappeared from the CV confirming a full coverage of all Au atoms by Pt atoms. At the same time, the currents in the H_{upd} potential region increase with increasing number of nominal Pt layers deposited. This indicates that the Pt layers are not deposited strictly layer by layer [6], but that they exhibit a certain roughness. This is also visible by the roughness factor. It increases from ca. 0.35 of the first nominal monolayer to slightly below 2 for the sample with 20 nominal monolayers.

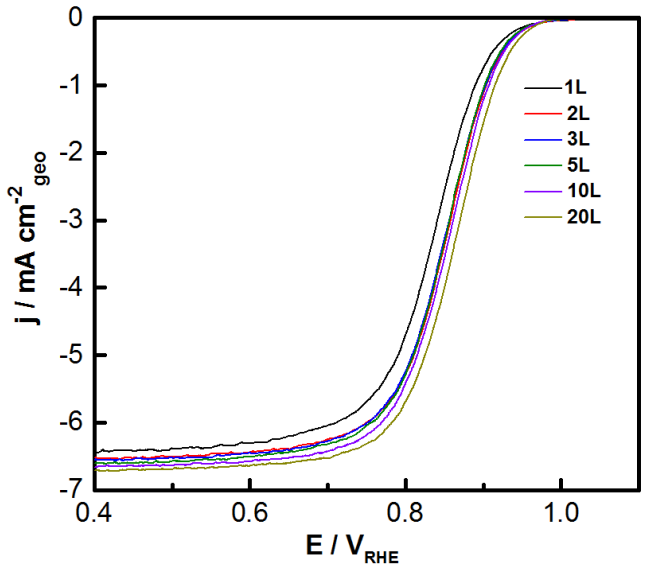

Figure 3. Positive going polarization curves of the PtAu-film electrodes with different amounts of nominal Pt layers; the scan speed was 50 mV/s, the electrolyte O_2 saturated 0.1M $HClO_4$ solution, and the rotation rate 1600rpm.

Figure 3 shows the test of the ORR activity of the PtAu-film electrodes with different amounts of nominal Pt layers. In all cases below 0.7 V_{RHE} a diffusion limited current plateau is seen, whereas between 0.8 and 1.0 V_{RHE} the mixed kinetic-diffusion limited potential region is observed. For the electrode with 1 nominal Pt layer, the diffusion limited current density j_d is slightly lower, which is in line with a lower geometric area of the Pt film due to incomplete coverage (the current is

normalized to the geometric area of the GC electrode). Alternatively, the lower diffusion limited current density might indicate incomplete oxygen reduction, i.e. the formation of hydrogen peroxide instead of water. However, such an interpretation would be in contrast to an increased ORR activity for this surface, see below. Upon deposition of the second Pt layer j_d only increases minimal as a result of increasing pseudocapacitance with increasing surface roughness. Furthermore, as the number of deposited Pt layers increases, the ORR curves shift to more positive potentials indicating an overall higher reaction rate.

In order to compare the site specific ORR rate, i.e. the specific activity (SA), we calculated the kinetic current density j_k from the measured current density j according to the well-known, Levich-Koutecky equation

$$\frac{1}{j} = \frac{1}{j_k} + \frac{1}{j_d} \qquad (1)$$

and normalized j_k to the Pt surface area established from the CVs shown in Figure 2. The resulting values for the SA as function of the number of nominally deposited Pt films is shown in Figure 4 for two potentials, 0.9 and 0.95 V_{RHE}, respectively.

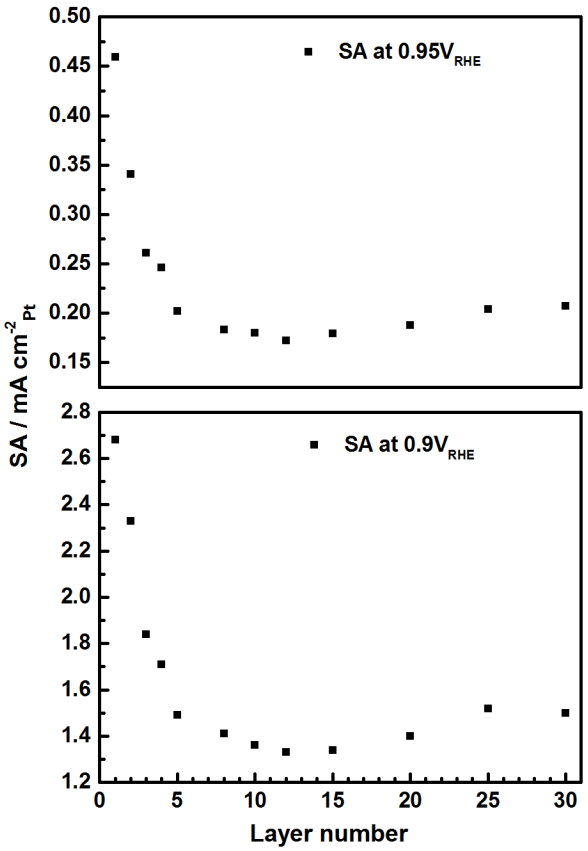

Figure 4. Comparison of the specific ORR activity SA at 0.9 and 0.95 V_{RHE} as a function of the number of nominal Pt layers deposited onto the Au-film electrodes.

Comparing the ORR SA at 0.9 and 0.95 V_{RHE} the following trend unfolds: the nominal Pt monolayer on Au exhibits the highest activity with 2.68 mA cm^{-2}_{Pt} at 0.9 V_{RHE}. With increasing number of deposited Pt layers the SA decreases below the value obtained for polycrystalline bulk Pt, that is while the second Pt layer (2.33 mA cm^{-2}_{Pt}) is still more active than polycrystalline bulk Pt, (1.72 mA cm^{-2}_{Pt}), the third and fourth nominal Pt layer exhibit approximately the Pt bulk activity (1.84 and 1.71 mA cm^{-2}_{Pt}). Interestingly, with additional Pt layer deposition, SA continues to decrease down to a value of ca. 1.3 mA cm^{-2}_{Pt} at 12 nominal monolayers, before rising again.

To better understand the observed activity trend we have carried out DFT calculations. We study activity by analyzing separately two regions in Figure 4; one at low Pt film thicknesses, corresponding to 1-2 nominal Pt layers, in which the thin films are more active than bulk Pt, and the

other at higher film thicknesses, where activity is lower or comparable to that of bulk Pt. Both regions provide hints on how different effects influence the ORR activity. To distinguish among different thin film formulations in the first region, we adopted the 1st layer/2nd layer composition nomenclature, where the composition in each layer is given by the number of atoms in the surface unit cell.

The ORR activity has been found in the past to follow a volcano-type relationship with respect to the binding energy of an arbitrarily chosen ORR intermediate [12,13]. Here, we use the potential, U, at which the surface starts to oxidize as the activity descriptor. U is the best descriptor in this case because it takes the minimum oxidation potential regardless of which species, OH or O is first formed (see the ESI for the calculation procedure). We have also computed hydrogen bonding corrections for adsorbed OH with water on different facets, by looking at different hydroxyl-water configurations (see the ESI). We find that for most of the (111) and all the (100) compositions, OH formation is more favorable than O formation. In contrast, on the Pt(110) surface water will almost always oxidize directly to O. Activities of thin films with the low Pt skin thickness are shown on the volcano plot in Figure 5, whereby the corresponding OH/O adsorption energies and oxidation potentials are compiled in Tables S1-6 in the ESI.

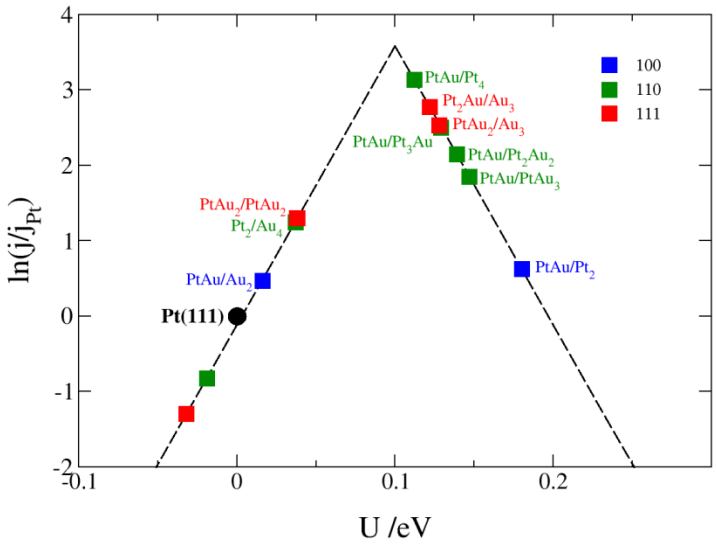

Figure 5. Activity estimates for ORR for Pt film thicknesses corresponding to 1-2 nominal layers as a function of the water oxidation potential.

For each surface termination there are certain configurations, mainly those with a (sub-) monolayer of Pt in the surface layer, that are active for ORR (see Fig. 5). Some of the present authors argued in a recent article that Au containing alloys most likely will not be active for ORR because of the large Au lattice constant;[14] however, here we see that there are some active formulations after all. It should be further noted that Au(100) is known to undergo reconstruction in an electrochemical environment [15] that results in growth of an epitaxially strained hexagonal surface layer. Therefore, we consider results on the non-reconstructed PtAu(100) thin films as approximate measures of ORR activity. It is noteworthy that we are able to reproduce activity trend for low-index Pt facets, Pt(100) < Pt(111) < Pt(110), which makes the calculations consistent with experiments.

In the following we will argue the importance of ligand, strain and ensemble effect on ORR activity. The strain effect originates from the Au lattice which is larger than the Pt lattice. Imposing a tensile strain on the surface makes the surface less active. That is, water oxidation products will bind more tightly to it. On the other hand, ligand effect exerts an opposite influence; nevertheless, in the cases where O formation is favorable, the ligand effect is not large enough to counteract strain. An additional requirement is to have surface Au, which occurs either at low deposited Pt coverage, or after enough time has elapsed for Au to segregate to the surface. Surface Au weakens the O binding energy through the ensemble effect. In the most stable adsorption configuration each O binds to three surface atoms on the Pt(111) and 1x2 reconstructed Pt(110) surface when adsorbed in a through position, and to two surface atoms on Pt(100). If one of these atoms is substituted by Au, the O binding becomes considerably weakened. Table 1 shows changes in the O binding energy when surface Pt atoms are consecutively replaced by Au.

To evaluate and quantify ligand and strain effect, Au layers have been successively substituted with Pt, starting from a 1ML Pt skin to a slab with only one Au layer. The corresponding changes in the OH/O binding energies and potentials are listed in Table 2. As can be noticed, the ligand effect is strongest when Au is present in the subsurface layer. As Au moves deeper beneath the surface the ligand effect lessens and already at 3-4 layers it completely vanishes. However, strain is still present in the layers where the ligand effect vanishes (compare binding energies of pure Pt and 5 layers thick Pt skin on Au). Thus, the activity will not directly decay to the value for bulk Pt as the number of Pt layers increases. In fact, it should first reduce below that value and then slowly converge towards it as the influence of strain weakens.

Table 1. O binding energies as a function of the number of Au atoms to which O binds.

facet	surface composition	ΔE(O) /eV
Pt(111)	Pt_3-Pt_3	1.022
	Pt_2Au-Pt_3	1.485
	$PtAu_2$-Pt_3	2.021
Pt(110)	Pt_2-Pt_4	1.253
	PtAu-Pt_4	1.747
	Au_2-Pt_4	2.189
Pt(100)	Pt_2-Pt_2	1.321
	PtAu-Pt_2	2.042

Table 2 Water oxidation potentials as a function of the Pt skin thickness.

Pt-skin	U_{111} /V	U_{110} /V	U_{100} /V
1-layer	0.618	0.823	0.218
2-layers	0.498	0.652	0.639
3-layers	0.579	0.604	0.467
4-layers	0.603	0.530	0.430
5-layers	0.628	0.584	0.459
∞-layers (pure Pt)	0.787	0.888	0.722

This type of behavior is clearly discernable in Figure 4, the activity is high at small Pt film thicknesses due to an interplay between ligand, strain and ensemble effect, then after ligand and ensemble effect die off, the remaining tensile strain renders Pt less active than bulk Pt. This gives rise to a small dip in activity at intermediate film thicknesses. After addition of more Pt layers, strain gradually vanishes and the activity finally approaches that of a bulk polycrystalline sample.

The problem with Au containing alloys is that Au has a very low surface energy, and thus energetically prefers to be at the surface. It is expected that the surface will become pure Au or highly Au enriched over time due to Au segregation. However, the effect can be reversed by oxygen induced Pt segregation at higher potentials (O favors Pt sites) [14]. Hence, in order to maintain active

compositions in fuel cells the potential needs to be cycled between potentials at which ORR operates and potentials at which lost Pt surface can be recovered.

4. Conclusions

We studied the ORR, the catalytic process occurring at the cathode in fuel cell, on Pt layers deposited onto Au. The nominal Pt layer by layer deposition reported in literature led to imperfect layers exhibiting a small number of uncovered Au atoms upon the first Pt layer deposition and a certain surface roughness with increasing number of Pt layers. This behavior might be associated with the roughness of the Au substrate. By probing the ORR it is seen, in contrast to previous predictions, that (sub-)monolayer amounts of Pt exhibit higher activity than Pt and that only for multilayers (> 2 nominal layers) the predicted ORR inhibition (decrease in activity as compared to bulk Pt) occurs. This behavior is explained by changes in the electronic structure brought by ligand, strain and ensemble effect as a function of the thin film thickness. At (sub-)monolayer coverage, the activity is governed by all three effects. For certain PtAu compositions ligand and ensemble effect lead to a weakening of the OH/O binding energy, suggesting that highly active sites are created by the Pt deposition. At larger film thicknesses, strain effect prevails leading to a decrease in the oxidation potential and activity. The results suggest that is possible to engineer PtAu core-shell nanoparticles with high catalytic. The challenge, however, will be to control the (near-)surface Au content and suppress further segregation, which is imminent in fuel cells due to the low Au surface energy.

Acknowledgment

Y-J.D. acknowledges funding from the China Scholarship Council (CSC). Furthermore we would like to acknowledge Markus Nesselberger and Xintai Wang for help concerning the preparation of the Au films and the AFM measurements respectively.

References

1. (a) Debe, M. K., Electrocatalyst approaches and challenges for automotive fuel cells. *Nature* **2012,** *486* (7401), 43-51; (b) Gasteiger, H. A.; Kocha, S. S.; Sompalli, B.; Wagner, F. T., Activity benchmarks and requirements for Pt, Pt-alloy, and non-Pt oxygen reduction catalysts for PEMFCs. *Appl Catal B-Environ* **2005,** *56* (1-2), 9-35.
2. Eberle, U.; Muller, B.; von Helmolt, R., Fuel cell electric vehicles and hydrogen infrastructure: status 2012. *Energ Environ Sci* **2012,** *5* (10), 8780-8798.
3. (a) Stamenkovic, V. R.; Mun, B. S.; Mayrhofer, K. J. J.; Ross, P. N.; Markovic, N. M., Effect of surface composition on electronic structure, stability, and electrocatalytic properties of Pt-transition metal alloys: Pt-skin versus Pt-skeleton surfaces. *J Am Chem Soc* **2006,** *128* (27), 8813-8819; (b) Wang, J. X.; Inada, H.; Wu, L. J.; Zhu, Y. M.; Choi, Y. M.; Liu, P.; Zhou, W. P.; Adzic, R. R., Oxygen Reduction on Well-Defined Core-Shell Nanocatalysts: Particle Size, Facet, and Pt Shell Thickness Effects. *J Am Chem Soc* **2009,** *131* (47), 17298-17302; (c) Xie, S. F.; Choi, S. I.; Lu, N.; Roling, L. T.; Herron, J. A.; Zhang, L.; Park, J.; Wang, J. G.; Kim, M. J.; Xie, Z. X.; Mavrikakis, M.; Xia, Y. N., Atomic Layer-by-Layer Deposition of Pt on Pd Nanocubes for Catalysts with Enhanced Activity and Durability toward Oxygen Reduction. *Nano Lett* **2014,** *14* (6), 3570-3576; (d) Chen, C.; Kang, Y. J.; Huo, Z. Y.; Zhu, Z. W.; Huang, W. Y.; Xin, H. L. L.; Snyder, J. D.; Li, D. G.; Herron, J. A.; Mavrikakis, M.; Chi, M. F.; More, K. L.; Li, Y. D.; Markovic, N. M.; Somorjai, G. A.; Yang, P. D.; Stamenkovic, V. R., Highly Crystalline Multimetallic Nanoframes with Three-Dimensional Electrocatalytic Surfaces. *Science* **2014,** *343* (6177), 1339-1343; (e) van der Vliet, D.; Wang, C.; Debe, M.; Atanasoski, R.; Markovic, N. M.; Stamenkovic, V. R., Platinum-alloy nanostructured thin film catalysts for the oxygen reduction reaction. *Electrochim Acta* **2011,** *56* (24), 8695-8699; (f) Stephens, I. E. L.; Bondarenko, A. S.; Gronbjerg, U.; Rossmeisl, J.; Chorkendorff, I., Understanding the electrocatalysis of oxygen reduction on platinum and its alloys. *Energ Environ Sci* **2012,** *5* (5), 6744-6762; (g) Greeley, J.; Stephens, I. E. L.; Bondarenko, A. S.; Johansson, T. P.; Hansen, H. A.; Jaramillo, T. F.; Rossmeisl, J.; Chorkendorff, I.; Norskov, J. K., Alloys of platinum and early transition metals as oxygen reduction electrocatalysts. *Nat Chem* **2009,** *1* (7), 552-556; (h) Gan, L.; Heggen, M.; Rudi, S.; Strasser, P., Core-Shell Compositional Fine Structures of Dealloyed PtxNi1-x Nanoparticles and Their Impact on Oxygen Reduction Catalysis. *Nano Lett* **2012,** *12* (10), 5423-5430; (i) Koh, S.; Strasser, P., Electrocatalysis on bimetallic surfaces: Modifying catalytic reactivity for oxygen reduction by voltammetric surface dealloying. *J Am Chem Soc* **2007,** *129* (42), 12624-+.
4. (a) Lefevre, M.; Proietti, E.; Jaouen, F.; Dodelet, J. P., Iron-Based Catalysts with Improved Oxygen Reduction Activity in Polymer Electrolyte Fuel Cells. *Science* **2009,** *324* (5923), 71-74; (b) Jaouen, F.; Herranz, J.; Lefevre, M.; Dodelet, J. P.; Kramm, U. I.; Herrmann, I.; Bogdanoff, P.; Maruyama, J.; Nagaoka, T.; Garsuch, A.; Dahn, J. R.; Olson, T.; Pylypenko, S.; Atanassov, P.; Ustinov, E. A., Cross-Laboratory Experimental Study of Non-Noble-Metal Electrocatalysts for the Oxygen Reduction Reaction. *Acs Appl Mater Inter* **2009,** *1* (8), 1623-1639.
5. (a) Kitchin, J. R.; Norskov, J. K.; Barteau, M. A.; Chen, J. G., Role of strain and ligand effects in the modification of the electronic and chemical properties of bimetallic surfaces. *Phys Rev Lett* **2004,** *93* (15); (b) Pedersen, M. O.; Helveg, S.; Ruban, A.; Stensgaard, I.; Laegsgaard, E.; Norskov, J. K.; Besenbacher, F., How a gold substrate can increase the reactivity of a Pt overlayer. *Surf Sci* **1999,** *426* (3), 395-409; (c) Naohara, H.; Ye, S.; Uosaki, K., Thickness dependent electrochemical reactivity of epitaxially electrodeposited palladium thin layers on Au(111) and Au(100) surfaces. *J Electroanal Chem* **2001,** *500* (1-2), 435-445.

6. Liu, Y.; Gokcen, D.; Bertocci, U.; Moffat, T. P., Self-terminating growth of platinum films by electrochemical deposition. *Science* **2012,** *338* (6112), 1327-30.
7. (a) Mayrhofer, K. J. J.; Wiberg, G. K. H.; Arenz, M., Impact of glass corrosion on the electrocatalysis on Pt electrodes in alkaline electrolyte. *J Electrochem Soc* **2008,** *155* (1), P1-P5; (b) Mayrhofer, K. J. J.; Crampton, A. S.; Wiberg, G. K. H.; Arenz, M., Analysis of the impact of individual glass constituents on electrocatalysis on pt electrodes in alkaline solution. *J Electrochem Soc* **2008,** *155* (6), P78-P81.
8. Mortensen, J. J.; Hansen, L. B.; Jacobsen, K. W., Real-space grid implementation of the projector augmented wave method. *Phys Rev B* **2005,** *71* (3).
9. Hammer, B.; Hansen, L. B.; Norskov, J. K., Improved adsorption energetics within density-functional theory using revised Perdew-Burke-Ernzerhof functionals. *Phys Rev B* **1999,** *59* (11), 7413-7421.
10. Monkhorst, H. J.; Pack, J. D., Special Points for Brillouin-Zone Integrations. *Phys Rev B* **1976,** *13* (12), 5188-5192.
11. (a) Snyder, J.; Danilovic, N.; Paulikas, A. P.; Tripkovic, D.; Strmcnik, D.; Markovic, N. M.; Stamenkovic, V. R., Thin Film Approach to Single Crystalline Electrochemistry. *J Phys Chem C* **2013,** *117* (45), 23790-23796; (b) Kim, J.; Lee, J.; Kim, S.; Kim, Y. R.; Rhee, C. K., Contrasting Electrochemical Behavior of CO, Hydrogen, and Ethanol on Single-Layered and Multiple-Layered Pt Islands on Au Surfaces. *J Phys Chem C* **2014,** *118* (42), 24425-24436.
12. (a) Rossmeisl, J.; Qu, Z. W.; Zhu, H.; Kroes, G. J.; Norskov, J. K., Electrolysis of water on oxide surfaces. *J Electroanal Chem* **2007,** *607* (1-2), 83-89; (b) Norskov, J. K.; Rossmeisl, J.; Logadottir, A.; Lindqvist, L.; Kitchin, J. R.; Bligaard, T.; Jonsson, H., Origin of the overpotential for oxygen reduction at a fuel-cell cathode. *J Phys Chem B* **2004,** *108* (46), 17886-17892.
13. Abild-Pedersen, F.; Greeley, J.; Studt, F.; Rossmeisl, J.; Munter, T. R.; Moses, P. G.; Skulason, E.; Bligaard, T.; Norskov, J. K., Scaling properties of adsorption energies for hydrogen-containing molecules on transition-metal surfaces. *Phys Rev Lett* **2007,** *99* (1).
14. Tripkovic, V.; Hansen, H. A.; Rossmeisl, J.; Vegge, T., First principles investigation of the activity of thin film Pt, Pd and Au surface alloys for oxygen reduction. *Phys Chem Chem Phys* **2015,** *17* (17), 11647-11657.
15. Ocko, B. M.; Wang, J.; Davenport, A.; Isaacs, H., Insitu X-Ray Reflectivity and Diffraction Studies of the Au(001) Reconstruction in an Electrochemical-Cell. *Phys Rev Lett* **1990,** *65* (12), 1466-1469.
16. Clay, C.; Haq, S.; Hodgson, A., Hydrogen bonding in mixed OH+H2O overlayers on Pt(111). *Phys Rev Lett* **2004,** *92* (4).
17. Markovic, N. M.; Ross, P. N., Surface science studies of model fuel cell electrocatalysts. *Surf Sci Rep* **2002,** *45* (4-6), 121-229.

Supporting information

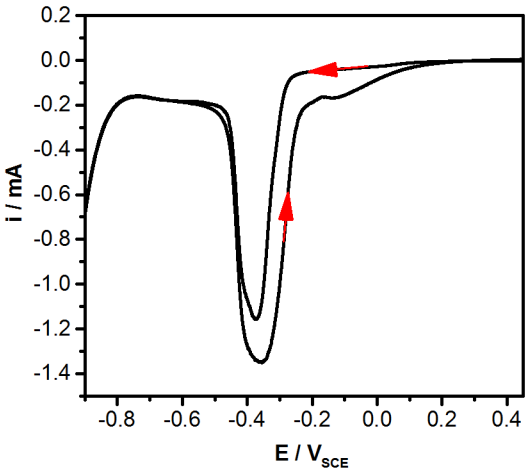

Figure S1. Cyclic voltammetry displaying Pt deposition from a pH 4.0 solution of 0.5 mol/L NaCl + 3 mmol/L K_2PtCl_4 (400 rpm, 2 mV/s). The reversible nature of suppressed and reactivated Pt deposition as previously reported can be observed.

Modelled surfaces

Illustrations of different surface terminations with the 1ML Pt skin are shown in Fig. S2.

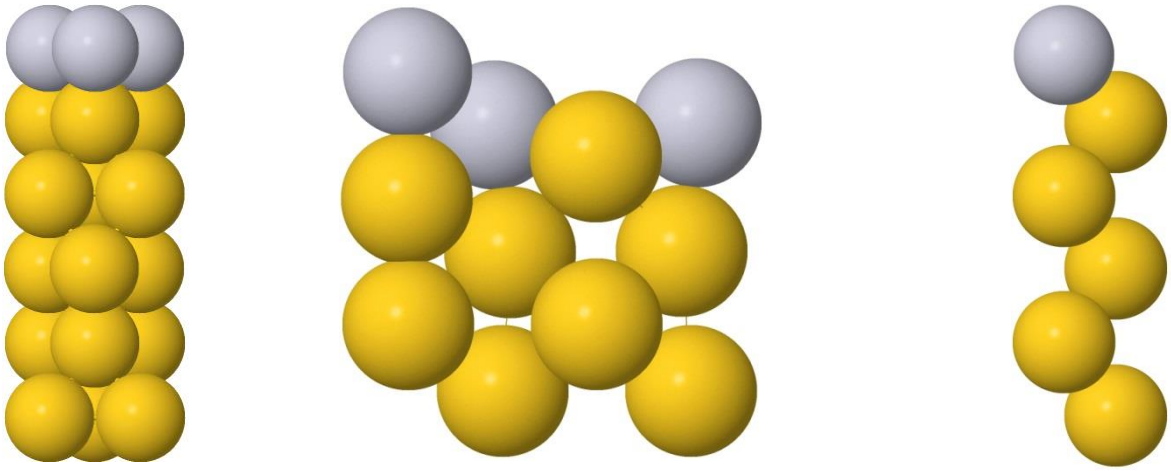

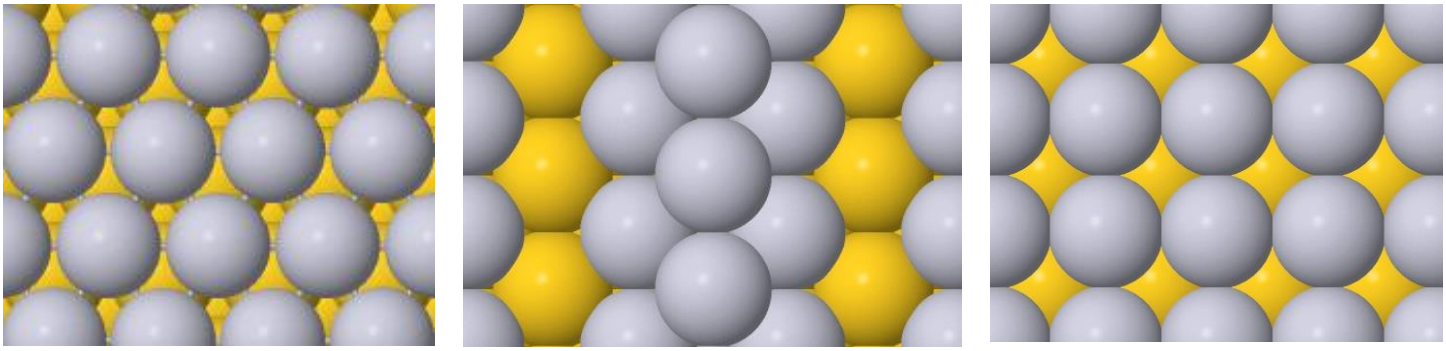

Figure S2. Side view (unit cell) and top views (repeated cell) of the simulated (111), (110) and (100) surfaces.

Calculating activity descriptor

The activity descriptor, U, is calculated in the following way:

$$U^{OH} = (E(OH^*) - E(*) - E(H_2O) + 1/2E(H_2) + ZPE - T\Delta S + E_{wc}$$

$$U^{O} = (E(O^*) - E(*) - E(H_2O) + E(H_2) + ZPE - T\Delta S$$

$$U = \min(U^{OH}, U^{O}),$$

where E(*), E(OH*) and E(O*) and are the total energies of the slab with and without OH or O adsorbates. E_{wc} is the water correction for OH species (see below), the hydrogen bonding between O and H_2O is too weak and can be neglected. Values for ZPE and entropy are taken from ref. [12b]. To get the water correction we have probed different OH-H_2O configurations for each crystal orientation. For the (111) plane, water correction is calculated for different Pt skin thicknesses (1-5 layers, including pure Pt as well) by having OH species in a half-dissociated water layer structure, which under UHV conditions at least, is the most stable hydroxyl-water arrangement on Pt(111) [16]. We take the average value by fitting a linear function through the different points (see Fig. S4). For the (110) surface the water correction has been calculated separately for OH adsorbed in an edge and through position. For the edge position the correction is 0.44 eV (1 ML point in Fig. S4) and for the through position approximately 0.15 eV. We used the through sites to measure the activity because it is believed that the edge sites are blocked by impurities [17]. No water correction has been

included for the (100) surface because by construction of the unit cell OH species make a hydrogen bonding chain that stabilizes adsorption energies by ca. 0.1 eV compared to isolated species.

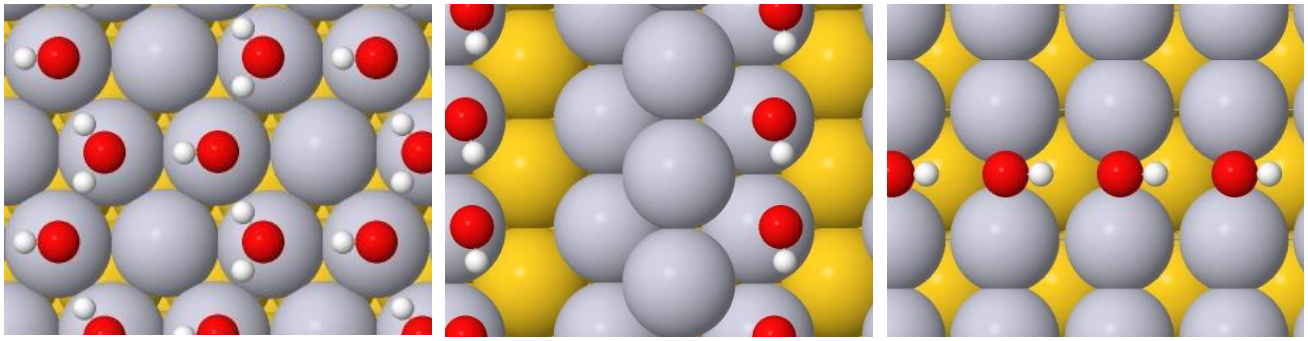

Figure S3 Top views of the most stable configurations of co-adsorbed water and hydroxyl species.

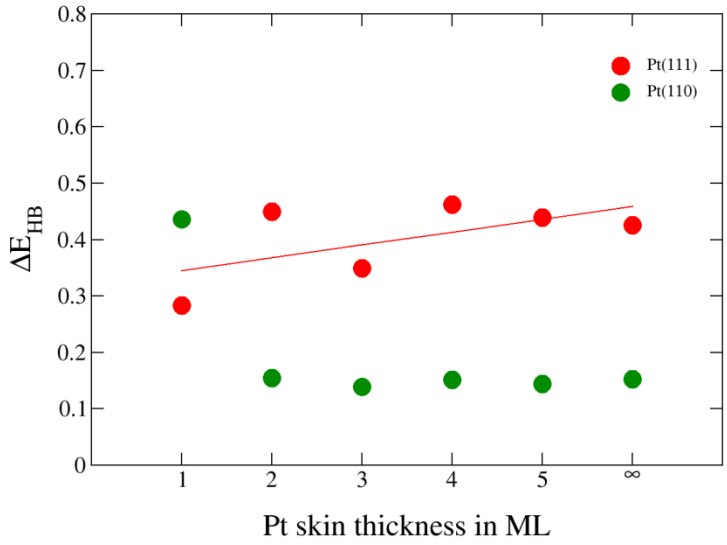

Figure S4. Corrections for hydrogen bonding interaction of OH with water.

Adsorption energies

If not stated otherwise the bulk material is Au.

Table S1. OH binding energy on different thin films with the (111) termination.

Alloy	ΔE(OH) /eV	U(OH) /V	ΔE(O) /eV	U(O) /V
Pt_3/Pt_3	0.598	0.504	1.022	0.536

Pt_2Au/Pt_3	0.622	0.533	1.485	0.768
$PtAu_2/Pt_3$	0.640	0.555	2.021	1.036
Pt_3/Pt_2Au	0.688	0.613	1.213	0.631
Pt_2Au/Pt_2Au	0.647	0.563	1.567	0.809
$PtAu_2/Pt_2Au$	0.725	0.658	2.208	1.129
$Pt_3/PtAu_2$	0.762	0.703	1.205	0.628
$Pt_2Au/PtAu_2$	0.806	0.755	1.721	0.886
$PtAu_2/PtAu_2$	0.864	0.825	2.331	1.191
Pt_3/Au_3	0.950	0.929	1.186	0.618
Pt_2Au/Au_3	0.960	0.941	1.780	0.915
$PtAu_2/Au_3$	0.932	0.908	2.334	1.192
Pure Pt	0.913	0.884	1.523	0.787

Table S2. OH binding energy as a function of the number of Pt layers in the Au(111) slab.

N-layers	ΔE(OH) /eV	U /V	ΔE(O) /eV	U /V
1	0.950	1.016	1.186	0.618
2	0.598	0.498	1.022	0.536
3	0.648	0.648	1.109	0.579
4	0.716	0.603	1.228	0.639

5	0.742	0.651	1.205	0.628
∞ (pure Pt)	0.913	0.884	1.523	0.787

Table S3. OH binding energy on different thin films with the (110) termination.

Alloy	ΔE(OH) /eV	U(OH) /V	ΔE(O) /eV	U(O) /V
Pt_2/Au_4	0.922	1.122	1.597	0.823
$PtAu/Au_4$	0.904	1.104	2.204	1.127
$Pt_2/PtAu_3$	1.169	1.369	1.326	0.688
$PtAu/PtAu_3$	1.111	1.311	1.817	0.934
$Au_2/PtAu_3$	1.076	1.276	2.254	1.152
Pt_2/Pt_2Au_2	1.263	1.463	1.485	0.768
$PtAu/Pt_2Au_2$	1.181	1.381	1.801	0.925
Au_2/Pt_2Au_2	1.151	1.351	2.122	1.086
Pt_2/Pt_3Au	1.215	1.415	1.253	0.652
$PtAu/Pt_3Au$	1.245	1.445	1.782	0.916
Au_2/Pt_3Au	1.171	1.371	2.082	1.066
Pt_2/Pt_4	1.199	1.399	1.253	0.652
$PtAu/Pt_4$	1.184	1.384	1.747	0.899
Au_2/Pt_4	1.142	1.342	2.189	1.120

Pure Pt	0.954	1.154	1.725	0.888

Table S4. OH binding energy as a function of the number of Pt layers in the Au(110) slab

N-layers	ΔE(OH) /eV	U /V	ΔE(O) /eV	U /V
2	1.199	1.399	1.253	0.652
3	0.955	1.155	1.158	0.604
4	0.792	0.992	1.010	0.530
5	0.773	0.973	1.117	0.584
∞ (pure Pt)	0.954	1.154	1.725	0.888

Table S5. OH binding energy on different thin films with the (100) termination.

Alloy	ΔE(OH) /eV	U(OH) /V	ΔE(O) /eV	U(O) /V
Pt_2/Pt_2	0.289	0.639	1.321	0.685
$PtAu/Pt_2$	0.617	0.967	2.042	1.046
$Pt_2/PtAu$	0.279	0.629	1.402	0.726
PtAu/PtAu	0.255	0.605	2.112	1.081
Pt_2/Au_2	-0.132	0.218	1.024	0.537
$PtAu/Au_2$	0.453	0.803	1.931	0.991
Pure Pt	0.372	0.722	1.420	0.735

Table S6 OH binding energy as a function of the number of Pt layers in the Au(100) slab.

N-layers	ΔE(OH) /eV	U /V	ΔE(O) /eV	U /V
1	-0.132	0.218	1.024	0.537
2	0.289	0.639	1.321	0.685
3	0.117	0.467	1.129	0.590
4	0.080	0.430	1.080	0.565
5	0.109	0.459	1.102	0.576
∞ (pure Pt)	0.372	0.722	1.420	0.735